Electrostatic Potential of B-DNA: Effect of Interionic Correlations

Sergei Gavryushov and Piotr Zielenkiewicz
Institute of Biochemistry and Biophysics, Polish Academy of Sciences, 02-106 Warszawa, Poland

ABSTRACT Modified Poisson-Boltzmann (MPB) equations have been numerically solved to study ionic distributions and mean electrostatic potentials around a macromolecule of arbitrarily complex shape and charge distribution. Results for DNA are compared with those obtained by classical Poisson-Boltzmann (PB) calculations. The comparisons were made for 1:1 and 2:1 electrolytes at ionic strengths up to 1 M. It is found that ion-image charge interactions and interionic correlations, which are neglected by the PB equation, have relatively weak effects on the electrostatic potential at charged groups of the DNA. The PB equation predicts errors in the long-range electrostatic part of the free energy that are only ~1.5 kJ/mol per nucleotide even in the case of an asymmetrical electrolyte. In contrast, the spatial correlations between ions drastically affect the electrostatic potential at significant separations from the macromolecule leading to a clearly predicted effect of charge overneutralization.

INTRODUCTION

Electrostatics of biological macromolecules has been a subject of continual interest through the years. Salt-dependent electrostatic effects are an important contributor to solvation and binding of charged macromolecules. Among others, DNA is one of the most important examples because of its singular biological role and, on the other hand, strongly exhibited polyelectrolyte properties in solution.

It is known that despite dramatic progress in Monte-Carlo (MC) and molecular dynamics (MD) simulations, the microscopic description of phenomena involving Coulombic forces meets serious difficulties. The large number of both water molecules and possible positions of free ions within the solvent makes such approaches practically impossible. According to recently reported MD simulations of DNA with ions (Young et al., 1997a,b), such studies are computationally very expensive, requiring several hundred hours of (CRAY C90) supercomputer time for each nanosecond of trajectory in the case of the DNA dodecamer duplex model. As a result, Poisson-Boltzmann (PB) calculations (Jayaram et al., 1989; Luty et al., 1992) and MC simulations (Lamm et al., 1994, Young et al., 1997a) based on continuum electrostatics remain the only generally applicable alternative. Although results of these calculations can be sensitive to the assumed geometry of the macromolecule, successful applications of the PB equation for the evaluation of the pK values of protein charged groups (Bashford and Karplus, 1990, 1991; Takahashi et al., 1992; Oberoi and Allewell, 1993; Loewenthal et al., 1993; Antosiewicz et al., 1994; Schaefer et al., 1997) show that the method correctly predicts salt-dependent free energies of ionization even for moderately concentrated solutions of electrolyte. Despite this, it should be taken into account that the PB equation is the simplest form of the double-layer statistical mechanical theory within the framework of the continuum solvent model (Carnie and Torrie, 1984). This equation ignores the finite size of ions and interionic spatial correlations, which reduce the range of ionic concentrations over which it can be applied. It also ignores repulsion between ions and their image charges, i.e., dielectric polarization forces acting on a single ion at the interface of water and a low dielectric constant medium (Carnie and Torrie, 1984). These forces take part in such phenomena as salting-out of proteins (Arakawa and Timasheff, 1985) and the increase in surface tension of electrolyte solutions (Carnie and Torrie, 1984).

Comparisons of PB calculations with MC simulations (Carnie and Torrie, 1984; Murthy et al., 1985; Mills et al., 1985; Degreve and Lozada-Cassou, 1995) have shown that for multivalent electrolytes the PB equation can produce large errors even at low ionic concentrations. Those comparisons were done for models of the simplest geometries. For more realistic models of DNA, such a comparison has shown a satisfactory agreement for diluted monovalent electrolyte and without image interactions of ions (Lamm et al., 1994). For diluted monovalent electrolyte, the PB equation was also experimentally verified by small-angle neutron scattering data for rod-like DNA fragments (Bhuiyan et al., 1996). The MC simulations for concentrated monovalent electrolyte (up to 2.5 M) showed phenomena such as the overneutralization of electrolyte around DNA (Montoro and Abascal, 1995), which entirely results from interionic correlations and cannot be produced by the PB equation in principle. The comparisons of MC with PB predictions for realistic models of DNA have not been extended to multivalent electrolytes.

In the present work the more advanced modified PB (MPB) equations are applied to the all-atom coordinates model of B-DNA, and results are compared with PB calculations. The basis of the MPB equations is the Kirkwood hierarchy of equations (Carnie and Torrie, 1984). The last is an exact formalism of statistical mechanics, which can be

Received for publication 30 December 1997 and in final form 31 August 1998.

Address reprint requests to Dr. Sergei Gavryushov, Institute of Biochemistry and Biophysics, Polish Academy of Sciences, Pawinskiego 5, 02-106 Warszawa, Poland. Tel.: 49-22-6584703; Fax: 48-39-121623; E-mail: serg@ibbrain.ibb.waw.pl.

0006-3495/98/12/2732/11 $2.00

applied to the electrical double layer. Being supplemented by a suitable closure approximation, these equations allow the effects of the finite size of ions and image forces to be incorporated into the theory. Starting from the work of Levine and Bell (1960; Bell and Levine, 1966) who considered a general form of short-range interactions between ions, the approach has been gradually developed through the years by Outhwhaite and Bhuiyan within the framework of the restricted primitive model (RPM) of electrolyte solutions. The last simplification means that ions are represented by hard spheres of equal diameter immersed in a continuous dielectric medium. The latter authors significantly refined the original theory and are responsible for a whole family of related theories: MPB1 through MPB5. The MPB equations based on the Kirkwood hierarchy and the linearized Loeb's closure (Carnie and Torrie, 1984) were formulated for planar (Levine and Outhwhaite, 1978), cylindrical (Outhwhaite, 1994), and spherical (Outhwhaite and Bhuiyan, 1991) double layers. The MPB equation can also be based on the Bogoliubov-Born-Green-Yvon (BBGY) hierarchy together with the linearized Loeb's closure. Such an approach was studied in the case of plane geometry (Outhwhaite, 1978). The two approximations lead to different equations for the same geometry. When neglecting ion size, the equations coincide as the weak-coupling theory for the point-ion model (Carnie and Torrie, 1984).

Although involving approximate solutions of the electrostatic boundary value problems, the MPB theory has been one of the most successful electrostatic double-layer theories for the RPM (see comparison with MC simulations in Carnie and Torrie, 1984, and Degreve and Lozada-Cassou, 1995). Precise quantitative agreement between the MPB and MC results is observed up to 2 M 1:1 electrolyte and 0.5 M 2:2 electrolyte (i.e., ionic strength of 2 M) at surface charges up to 0.15 C m^{-2}, whereas PB results are correct up to 0.1 M 1:1 electrolyte and surface charges up to 0.044 C m^{-2} (Carnie and Torrie, 1984). Moreover, the MPB theory incorporates the charge-image interactions in a more natural way than any current theory of the electrical double layer. These forces are not central, which makes, for example, MC simulations with image forces to be computationally very expensive. The impossibility of applying approximate solutions of involved electrostatic boundary value problems to a more complex geometry has prevented a more widespread appreciation of the MPB theory.

Recently we reported the full numerical implementation of an approach based on the BBGY equations which, together with the linearized Loeb's closure, were programmed for an arbitrarily complex macromolecule and applied to study the salt dependence of a protein's free energy (Gavryushov and Zielenkiewicz, 1997b). In the present work the same program, rewritten for the Kirkwood equations, is used for calculations of the mean electrostatic potential and ionic distributions around an all-atom model of B-DNA. The subject of interest is the difference between PB and MPB electrostatic potentials around charged groups of DNA. Because of the above mentioned errors in the PB approximation in the case of multivalent electrolytes, the comparison is done for 1:1 and 2:1 diluted electrolytes. The sensitivity of results to such adjustable parameters as the size of ions and the dielectric constant of the DNA's interior is also studied. Such effects as dielectric saturation, the dependence of the solvent dielectric constant on the ionic concentrations (Lamm and Pack, 1997), and the polarization of ions are not considered, although they can be approximately incorporated into the MPB equations (Levine and Bell, 1960; Bell and Levine, 1966). In other words, uniform although different dielectric constants are used for both the interior of the macromolecule and the surrounding solvent. The free energy dependence on ionic concentration is not evaluated here, although there have been attempts to apply such solvent continuum-based methods as the potential mean force (PMF) approach (Soumpasis, 1984) or the PB equation (Misra and Honig, 1996) to the B-Z DNA transition free energy, as well as studies of PB-calculated salt effects on protein-DNA binding free energies (Misra et al., 1994a). As follows from a comparison of BBGY calculations of the lysozyme free energy dependence on salt concentration with experimental data, the RPM for electrolyte is inadequate even at moderate dilution of electrolyte. The solvent forces acting on ions within inner coordination shells of solvent molecules drastically contribute to the free energy dependence on salt concentration. Although correctly reproducing mean electrostatic potentials at charged groups (and, consequently, the pK values of their ionization), the solvent continuum model should not be applied to macromolecular transfer between two media at salt concentrations higher than ~0.1 M (Gavryushov and Zielenkiewicz, 1997b). One should also be careful if macromolecular aggregation is accompanied by a significant change of the solvent accessible surface. It should be noted that successful PB calculations of the experimentally observed binding constants for DNA-binding proteins (Misra et al., 1994a; Zacharias et al., 1992) have been reported for diluted 1:1 electrolyte (salt concentration, ≤0.1 M). In contrast, successful PB binding free energy calculations at higher salt concentrations were carried out for small ligands (Misra et al., 1994b; Misra and Honig, 1995). In both cases the above mentioned effect is negligible. As a result, we concentrate our study only on mean electrostatic potential evaluations and avoid the DNA free energy dependence on salt concentration.

THEORY

The Kirkwood hierarchy together with linearized Loeb's closure gives the following equations for distribution of ions of species α, represented by hard spheres of diameter d (Carnie and Torrie, 1984):

$$\ln g_\alpha(\mathbf{r}) = \ln \xi_\alpha(\mathbf{r}) - \beta q_\alpha \psi(\mathbf{r}) - \beta q_\alpha \int_0^1 d\lambda \{\eta_\alpha(\mathbf{r}|\lambda) - \eta_\alpha(\infty|\lambda)\}, \quad (1)$$

where $\beta = 1/kT$, q_α is the charge of an ion, $\psi(\mathbf{r})$ is the mean electrostatic potential, and the mean ionic concentration $n_\alpha(\mathbf{r})$ is expressed via the ionic bulk concentration n_α^0 and the distribution function $g_\alpha(\mathbf{r})$ as $n_\alpha(\mathbf{r}) = n_\alpha^0 g_\alpha(\mathbf{r})$. The right side of Eq. 1 is the potential of mean force (PMF) acting on the ion, divided by $-kT$. In case of the PB approximation, it is reduced to the second $q_\alpha\psi(\mathbf{r})$ term. The first term of the PMF appears due to the work required to insert an uncharged ion at point $\mathbf{r}$ and is denoted as $-kT\ln\xi_\alpha(\mathbf{r})$. This so-called exclusion volume term obviously vanishes for point-like ions. The third term of the PMF is due to the difference between an ion's self-atmosphere energies at position $\mathbf{r}$ and at infinity, ion-image interactions, and the work of diffuse charge distribution removal from the spherical exclusion volume of the ion. It is important to note that the self-atmosphere and ion-image forces remain even for the point-like ion model. The physical meaning of the self-atmosphere effect is apparent if one considers a symmetrical electrolyte close to the uncharged surface. In this region the Debye-Huckel atmosphere of opposite charge surrounding each ion becomes unsymmetrical, and so causes a small extra repulsion of ions from the surface. On the other hand, the mean electrostatic potential is zero due to the charge symmetry of the system, and thus the PB approximation is not able to describe the effect. Similarly, the PB equation cannot describe ion-image interactions, i.e., long-range polarization forces acting on charges in a nonuniform dielectric. For example, such electrostatic forces take part in repulsion of both anions and cations from the air-water interface, despite a zero mean potential in the case of symmetric electrolytes.

The Kirkwood hierarchy of equations is derived by introducing a coupling constant λ that couples one ion of species α with the rest of the system. In case of the MPB theory, this procedure corresponds to charging an ion, which yields an equation for $\eta_\alpha(\mathbf{r}|\lambda)$:

$$\eta_\alpha(\mathbf{r}_2|\lambda) = \lim_{\mathbf{r}_1\to\mathbf{r}_2}\left[\phi_\alpha(\mathbf{r}_1, \mathbf{r}_2|\lambda) - \frac{\lambda q_\alpha}{\epsilon_W r_{12}}\right], \qquad (2)$$

where ϵ_W is the solvent dielectric constant, $q_\alpha/(\epsilon_W r_{12})$ is the Coulombic self-potential of the ion, and $\phi_\alpha(\mathbf{r}_1, \mathbf{r}_2|\lambda)$ is the fluctuation potential. The last satisfies the following equations for the RPM (Carnie and Torrie, 1984):

$$\nabla_1^2\phi_\alpha(\mathbf{r}_1, \mathbf{r}_2|\lambda) = 0 \qquad (3.1)$$

(inside the macromolecule's interior and the shell of ionic exclusion around the macromolecule)

$$\nabla_1^2\phi_\alpha(\mathbf{r}_1, \mathbf{r}_2|\lambda) = -\nabla_1^2\psi(\mathbf{r}_1) - \frac{4\pi}{\epsilon_W}\lambda q_\alpha\delta(\mathbf{r}_1 - \mathbf{r}_2) \qquad (3.2)$$

(within the ionic atmosphere around the macromolecule, $r_{12} < d$)

$$\nabla_1^2\phi_\alpha(\mathbf{r}_1, \mathbf{r}_2|\lambda) = k^2(\mathbf{r}_1)\phi_\alpha(\mathbf{r}_1, \mathbf{r}_2|\lambda) \qquad (3.3)$$

(within the ionic atmosphere around the macromolecule, $r_{12} > d$), where

$$k^2(\mathbf{r}) = \frac{4\pi\beta}{\epsilon_W}\sum_\gamma n_\gamma(\mathbf{r})q_\gamma^2.$$

Equations 3.1–3.3 are subject to the boundary conditions on the surface of the macromolecule:

$$\phi_\alpha|_{\text{inside}} = \phi_\alpha|_{\text{outside}}$$
$$\epsilon\frac{\partial\phi_\alpha}{\partial n}|_{\text{inside}} = \epsilon_W\frac{\partial\phi_\alpha}{\partial n}|_{\text{outside}}, \qquad (4)$$

where ϵ is the dielectric constant of the macromolecule's interior. The mean electrostatic potential $\psi(\mathbf{r})$ from Eq. 1 satisfies the Poisson equation:

$$\nabla^2\psi(\mathbf{r}) = -\frac{4\pi}{\epsilon}\rho_0(\mathbf{r}) \qquad \text{inside the macromolecule,}$$
$$\nabla^2\psi(\mathbf{r}) = -\frac{4\pi}{\epsilon_W}\sum_\gamma q_\gamma n_\gamma(\mathbf{r}) \qquad \text{outside the macromolecule,} \qquad (5)$$

where ρ_0 is the charge density of the macromolecule. As for the fluctuation potential, the boundary conditions for $\psi(\mathbf{r})$ on the macromolecule's surface require continuity in ψ and in its normal derivative multiplied by the dielectric constant of the medium. At low ionic concentrations, the exclusion volume term $\ln\xi_\alpha(\mathbf{r}_2)$ may be approximated by $-\int_{V_\alpha}\Sigma_\gamma(n_\gamma(\mathbf{r}) - n_\gamma^0)d^3\mathbf{r}$ (Bell and Levine, 1966), where $V_\alpha = (4/3)\pi d^3$ is the excluded volume of a small ion of diameter d centered at position $\mathbf{r}_2$. This is just the work against the osmotic pressure of an ionic gas that is considered as perfect.

By neglecting the first and third terms of the right part of Eq. 1 and substituting into Eq. 5, Eq. 5 becomes the PB equation. Its solution gives an initial estimate of $\psi^{(0)}(\mathbf{r})$, which makes it possible to obtain $\phi_\alpha^{(0)}(\mathbf{r}_1, \mathbf{r}_2)$ through Eq. 3. Then one obtains $g_\alpha^{(1)}(\mathbf{r})$ through Eq. 1 and $\psi^{(1)}(\mathbf{r})$ through Eq. 5 and so on. This iterative procedure was applied to a highly charged cylindrical polyion, where a very fast convergence of loop (5)-(3)-(1)-(5) was observed (Gavryushov and Zielenkiewicz, 1997a).

METHOD

The finite-difference (FD) implementation of three-dimensional (3D) Eqs. 1–5 has been described in the previous work (Gavryushov and Zielenkiewicz, 1997b). The main difficulty in solving Eqs. 2 and 3 numerically originates from the singularity of the fluctuation potential $\phi(\mathbf{r}_1, \mathbf{r}_2)$ at $\mathbf{r}_1 \to \mathbf{r}_2$ and from the nature of Eq. 3, which has to be solved at all positions of points $\mathbf{r}_2$ around the macromolecule. The last requires a giant amount of computation and, consequently, the choice of nonuniform net of $\mathbf{r}_2$ points becomes crucial. Assigning the δ-function position to the lattice

node, we use the following method to solve the singularity problem:

$$\int_0^1 d\lambda\{\eta_\alpha(\mathbf{r}|\lambda) - \eta_\alpha(\infty|\lambda)\} \approx \frac{1}{2}[\phi_\alpha^\delta(\mathbf{r}, \mathbf{r}|1) - \phi_\alpha^\delta(\infty|1)] + (\phi_\alpha^\psi(\mathbf{r}, \mathbf{r}) - \phi_\alpha^\psi(\infty)),$$

where $\phi_\alpha^\delta(\mathbf{r}_1, \mathbf{r}_2|\lambda)$ and $\phi_\alpha^\psi(\mathbf{r}_1, \mathbf{r}_2)$ are numerical solutions corresponding to the two terms on the right side of Eq. 3.2. Tests show that the difference $\phi_\alpha^\delta(\mathbf{r}_1, \mathbf{r}_1) - \phi_\alpha^\delta(\mathbf{r}_2, \mathbf{r}_2)$ does not depend on lattice spacing to solve Eq. 3 and thus can produce correct results.

A nonuniform distribution of $\mathbf{r}_2$ points is used. The macromolecule, together with the zone excluded to ions, is surrounded by three layers of δ-function positions. The first, inner, layer has a thickness approximately half the Debye-Huckel length λ_{DH} for the bulk electrolyte. The others are of thickness λ_{DH}. Every point of the FD grid for Eq. 5 is taken as a point $\mathbf{r}_2$ for Eq. 3 within the first layer. The nodes of this grid are also taken as points $\mathbf{r}_2$ within other layers with a doubled spacing for the second layer and a four times larger spacing for the third one. The external part of $\mathbf{r}_2$ points is distributed with eight times larger spacing. This method allows the number of numerical solutions of Eq. 3 to be reduced to several thousands, and thus makes the numerical solution of system (1)-(5) practically possible. An important feature of the algorithm is that all Eqs. 3 can be solved in parallel within one loop (5)-(3)-(1)-(5).

Another problem is the 3D interpolation of the η function to be calculated via Eq. 2 for all points of the regular FD grid for Eq. 5. This function is not determined within the macromolecule's interior, which leads to a complicated code because of the arbitrary shape of the macromolecule. The interpolation is based on the η function gradient least-squares approximation. The method is exact for a linear function. Equation 5 is numerically solved in the same way as the quite similar nonlinear PB equation (Jayaram et al., 1989). The sizes of the FD grid for Eq. 5 are determined so that the minimal distance between the ion-accessible surface of the macromolecule and the outer boundary of the grid is several λ_{DH}. The last value was taken as $3\lambda_{DH}$ at low ionic strengths ($I < 0.5$ M) and as $5\lambda_{DH}$ at $I > 0.5$ M. For the model of DNA, periodic boundary conditions on the z axis are applied. The macromolecule is described at the all-atom coordinates level. Charges are assigned to the center of each atom. The values of these charges are taken from the AMBER force field (Weiner et al., 1984).

Testing

The numerical algorithm for the BBGY equations has been tested previously on cylindrical models (Gavryushov and Zielenkiewicz, 1997a) where data of MC simulations are published in the literature (Das et al., 1995). Corresponding calculations based on the Kirkwood equations demonstrate similar or even better agreement with MC simulations (data not published). Numerical solutions of 3D Eqs. 1–5 were compared with MC simulated data for spherical geometry. Those data were taken from the work by Degreve and Lozada-Cassou, 1995. The model is a 15-Å-radius highly charged spherical macro-ion immersed in an asymmetric RPM electrolyte at 0.005 and 0.5 M concentrations. The hard sphere diameter for all salt ions is taken as 4 Å. The divalent counterion model was explored as the PB equation fails quantitatively in this case (see Fig. 3 of the work by Degreve and Lozada-Cassou, 1995). A $75 \times 61 \times 61$ point grid was used to solve Eq. 3, which corresponds to a lattice spacing of 3.05 Å at 0.005 M and of 0.81 Å at 0.5 M. The MPB electrostatic potential on the ion-accessible surface of the macroparticle is in agreement with the published MC data and results of more advanced MPB5 theory for the spherical geometry within accuracy of 5–15%.

The 3D algorithm was also intensively tested on the cylindrical polyion model where the one-dimensional (1D) Runge-Kutta solution of Eq. 5 can be independently obtained. The parameters of the model were taken close to the cylindrical approximate model of the DNA molecule represented by a linear lattice of negative charges placed 1.7 Å apart on the axis of an 8-Å-radius cylinder. The dielectric constant of the polyion is 2, the solvent dielectric constant is 80. Comparisons of 3D and 1D results are shown in Fig. 1 for two ionic strengths of 2:1 RPM electrolyte: $I = 0.05$ M and $I = 0.5$ M where all counterions (cations) are divalent. To obtain 3D solutions of Eq. 5, the 8-Å-radius polyion and a region of surrounding solvent are mapped onto a $53 \times 53 \times 25$ point lattice at $I = 0.05$ M and onto a $97 \times 97 \times 33$ point lattice at $I = 0.5$ M. The corresponding resolutions are 0.5 grid/Å and 2 grid/Å, respectively. Both the hard sphere radius for ion-ion interactions and the ion exclusion radius are taken as 2 Å. In the case of the 3D solutions, the resulting numbers of $\mathbf{r}_2$ points (i.e., numbers of Eqs. 3 to be solved numerically) are ~6000 and 29,000, respectively. There are only ~30 $\mathbf{r}_2$ points lying on the radial line in the case of 1D solutions. Results for 1D and 3D solutions of the PB equation are also shown in Fig. 1. An excellent agreement between 1D and 3D results suggests that the method of distributing points $\mathbf{r}_2$ is correct in the case of the model with parameters taken close to those of the model of DNA.

RESULTS AND DISCUSSION

The B-DNA duplex of sequence $d(CG)_5$ (one complete turn) was chosen to compare the PB and MPB mean electrostatic potentials and ionic distributions. The calculations were carried out for several ionic strengths of 1:1 and 2:1 RPM electrolytes. Results for moderately diluted electrolyte seem to be most interesting. Here we present data obtained at ionic strengths $I = 0.5$ M ($C_{1:1} = 0.5$ M, $C_{2:1} = 0.167$ M, $\lambda_{DH} = 4.34$ Å) and $I = 1$ M ($C_{1:1} = 1$ M, $C_{2:1} = 0.33$ M, $\lambda_{DH} = 3.07$ Å). Results for diluted electrolytes ($I = 0.05$ M)

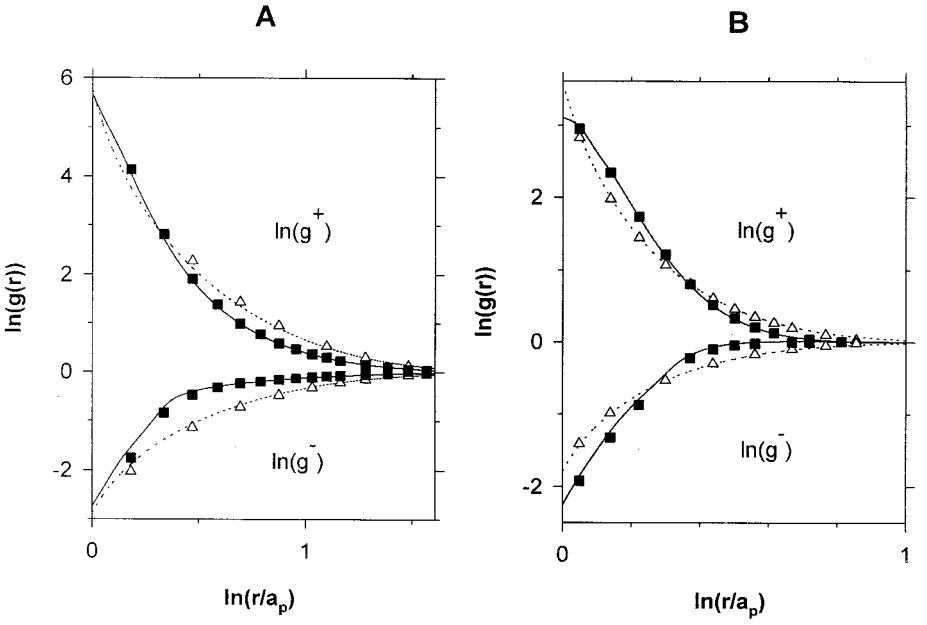

FIGURE 1 Comparison of 1D with 3D technique calculated ionic distributions around a cylindrical polyion: a_p = 10 Å; 2:1 electrolyte at ionic strengths I = 0.05 M (*A*) and I = 0.5 M (*B*); ion diameter is 4 Å; internal dielectric constant is set to 2; the solvent dielectric constant is 80. —, 1D MPB calculations; ■, 3D MPB results; – – – and △, 1D and 3D PB results, respectively.

are also discussed. Other parameters of the model are as follows. The hard sphere diameter for the ion-ion short-range interaction is taken as 4 and 6 Å for comparison. The ionic exclusion radius $\boldsymbol{r}_{excl}$ around the molecule of DNA is also considered as a variable parameter. The values of 2 and 3 Å are applied. The solvent dielectric constant is set to 80, the DNA's interior dielectric constant is taken as 10 (also 80 for comparison). The all-atom model of the DNA dodecamer is mapped onto a 69 × 69 × 41 point lattice at I = 0.5 M and an 85 × 89 × 49 point lattice at I = 1 M (the z axis corresponds to the helical axis of DNA). The lattice spacings are 0.845 and 0.704 Å, respectively. The system of Eqs. 1–5 was solved with periodic boundary conditions applied to the z axis for Eq. 5. The x-y boundary value of the potential is zero. Corresponding numbers of Eqs. 3 within one loop (5)-(3)-(1)-(5) are approximately 19,900 and 24,000. The convergence of this main cycle is so fast that only two to three iterations are needed. As a result, the electrostatic potential is calculated in a few hours on 16 processors of the CRAY T3E supercomputer.

Results for the model described above are shown in Figs. 2–7 as mean electrostatic potential contour maps in a midplane slice perpendicular to the helix axis and as 1D plots of potentials and ionic distributions. The plane is the same for all pictures (except for Fig. 4) and it is taken close to the charged phosphate groups of DNA. All 1D profiles are taken along the same direction (1,2), marked in Fig. 2, across the middle of the major groove and helical axis of DNA. In Figs. 2 *A* and 3 *A*, results for a 0.5 M 1:1 electrolyte are shown. A reasonable agreement between the PB potential and the MPB potential (d_{ion} = 4 Å) is clearly observed. The difference $\psi_{MPB} - \psi_{PB}$ on the solvent-accessible surface is less than 0.5 in kT/e units. It confirms the well known fact that the PB equation correctly describes diluted 1:1 electrolyte double layers. Figs. 2 *A* and 3 *A* also demonstrate sensitivity of the mean electrostatic potential to the hard sphere diameter of ions. The difference between ψ_{MPB} and ψ_{PB} becomes higher and reaches 0.75 kT/e when d_{ion} = 6 Å is used instead of 4 Å (the radius of ion exclusion on the surface of the molecule is fixed at 3 Å). A new phenomenon is also observed. One can see a zero potential contour; i.e., the electrostatic potential becomes positive in the external area. In other words, the ionic cloud not only compensates for all the polyelectrolyte charge but even exceeds it at some distance from the macromolecule's surface. This overneutralization is described in the literature for polyelectrolyte systems and, in particular, for MC simulations of ion distributions around DNA models (Montoro and Abascal, 1995; Das et al., 1997). As mentioned in those works, the effect originates from the spatial ion-ion correlations; the PB equation, which neglects such correlations, never gives any charge inversion, irrespective of the concentration of added salt.

The charge reversal effect is strongly exhibited at higher ionic concentrations and for 2:1 electrolyte. The difference between ψ_{MPB} and ψ_{PB} is notable in the case of 1 M 1:1 electrolyte; on the solvent-accessible surface it reaches 0.5 kT/e or ~30% of the potential value even at d_{ion} = 4 Å (which corresponds to the diameter of a hydrated sodium ion). A comparison of the PB and MPB electrostatic potentials for 2:1 electrolyte is shown in Figs. 2 *B* and 3 *B*. Counterions are divalent. One can see that the effect of the charge overneutralization is more pronounced than in the case of monovalent electrolyte. At d_{ion} = 6 Å areas of relatively high positive electrostatic potential ($\psi_{MPB} > +0.5\ kT/e$) appear at a several angstrom units separation from the solvent-accessible surface. On the surface, the difference between ψ_{MPB} and ψ_{PB} reaches ~1 kT/e even at I = 0.5 M (C = 0.167 M) and d_{ion} = 4 Å, which is 40% of the magnitude. The difference is higher if d_{ion} = 6 Å is

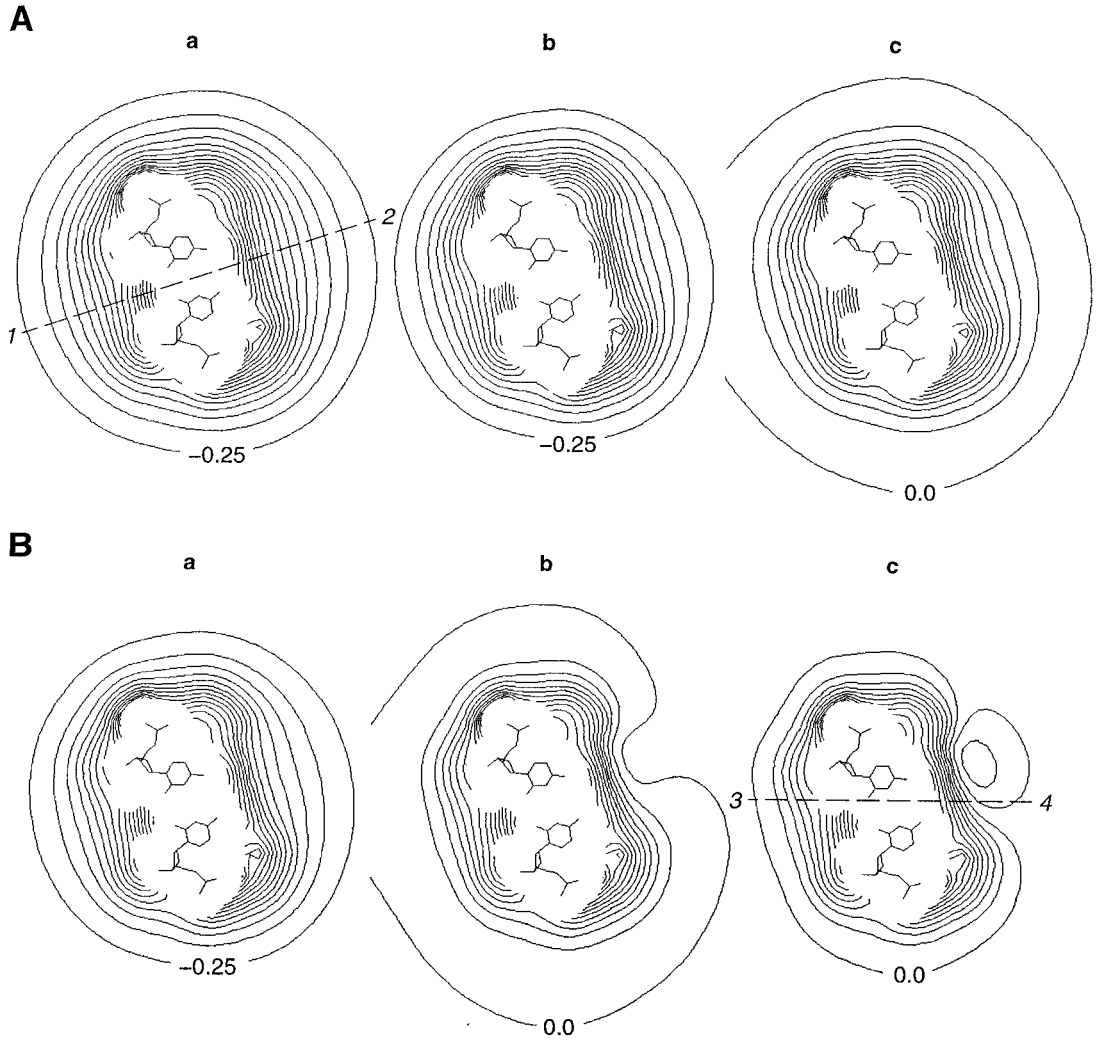

FIGURE 2 Contour maps of the electrostatic potential in the solvent-accessible area around the all-atom model of DNA. Contours are taken with 0.25 kT/e difference. Monovalent (*A*) and 2:1 (*B*) electrolytes; $I = 0.5$ M; $r_{excl} = 3$ Å. The DNA's interior dielectric constant is set to 10; the solvent dielectric constant is 80. (*a*) PB equation; (*b*) MPB equations, $d_{ion} = 4$ Å; (*c*) MPB equations, $d_{ion} = 6$ Å.

used. A similar picture is observed for the doubled concentration of ions. At $I = 1$ M ($C = 0.33$ M) the corresponding difference is ~0.75 kT/e, or 40% of magnitude. At $d_{ion} = 6$ Å, the relative errors of ψ_{PB} are estimated as ~70%. The electrostatic potential maximum appears close to the major groove of DNA as one can see from the potential contour map in a plane slice across the helical axis (Fig. 4). The map corresponds to the model shown in Fig. 2 *Bc* (where the vertical plane is marked by line (3,4)). Another area of positive mean potential appears along the minor groove in the case of 1 M 6-Å multivalent electrolyte (data not shown). The ionic distributions also clearly exhibit the charge overneutralization effect. One-dimensional profiles of cation and anion distributions for 2:1 electrolyte at $I =$ 0.5 M and $I = 1$ M are shown in Fig. 5. Numerical artifacts of the η function 3D interpolation may be seen as slight steps in the curves at long distances from the surface of DNA.

The correctness of the calculations was checked by a change of the grid spacing, increase of the thickness of the inner layer of singularity positions, and radial increase of the grid sizes. The η function and electrostatic potential were found to be stable. For example, a change of the minimal distance between the ion-accessible surface of DNA and the outer boundary of the grid from $3\lambda_{DH}$ to $5\lambda_{DH}$ affects the magnitudes of ψ within 1–2%. Doubling of the thickness of the inner layer of the singularity positions leads to a significantly higher number of Eqs. 3 to be solved. At $I = 0.5$ M, it results in ~37,000 Eqs. 3 instead of 19,900. Comparisons of results show that both the electrostatic potential and the η function are invariant to this expansion. A several percent difference in the potentials is observed only at a significant separation from the surface of DNA, where the absolute value of ψ is much lower than 0.1 kT/e. Results are also invariant to the decrease of the grid spacing. For example, MPB electrostatic potentials are stable within

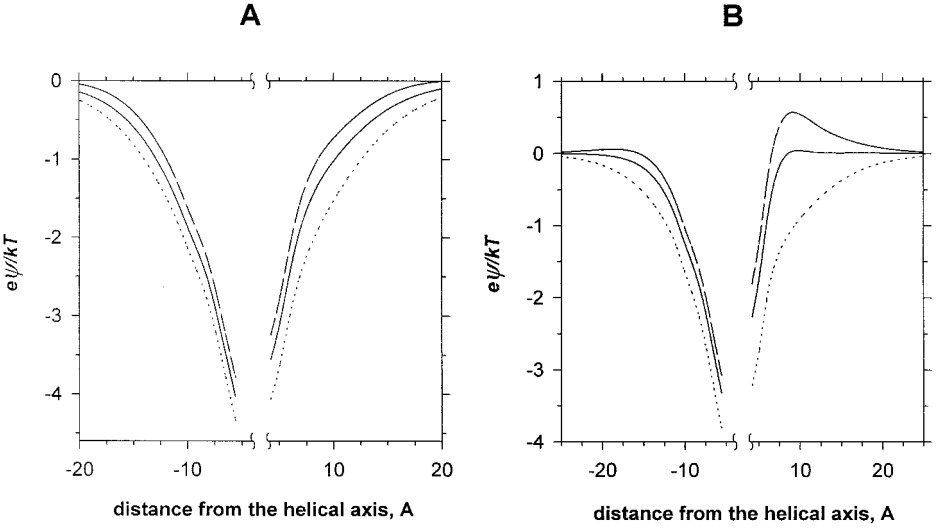

FIGURE 3 Electrostatic potential plots corresponding to potential contour slices shown in Fig. 2. (*A*) 1:1 electrolyte; (*B*) 2:1 electrolyte. Profiles are taken along line (1,2) marked in Fig. 2. The dotted curves are solutions of the PB equation; the solid and dashed curves are MPB results for d_{ion} = 4 Å and d_{ion} = 6 Å, respectively.

a few percent if the grid spacing is taken as 0.6 Å instead of 0.845 Å at I = 0.5 M. A relatively higher instability of the potential is only observed close to the positive potential maximum for a d_{ion} = 6 Å model (up to 10%). The magnitude of the total ionic charge surrounding the macromolecule is in agreement with the total charge of DNA with an accuracy of 1–2%. This reflects the accuracy of the FD approximation of Eq. 5, which follows from the fact that this discrepancy is reduced together with decrease of the grid spacing. (The same accuracy of 3D solutions of Eq. 5 is found from comparisons of 3D with 1D PB potentials for the cylindrical model.) It is important to note that numerical errors in the total ionic charge are not changed at the expansion of the outer boundary surface, described above. This can be regarded as a justification of the outer boundary conditions chosen for both the PB and MPB equations.

In the case of 1 M ionic strength electrolytes, the electrostatic potential is sensitive not only to short-range ionic interactions but also to the thickness of the ionic exclusion zone (the Stern layer) around the macromolecule. Strong polarization forces must affect ions within the inner coordination shell of water molecules, repelling ions from the macromolecule's atoms. (Such forces cause the electrical dissociation of salt in water by repelling oppositely charged ions each from other.) Because the geometry of the macromolecule's surface differs from the surfaces of two ions, the effective ionic exclusion radius may differ from the parameter that pertains to ion-ion interactions. In other words, the thickness of the Stern layer should be considered as an independent parameter of the model. The MPB electrostatic potentials were compared for r_{excl} = 3 Å and r_{excl} = 2 Å (the model of 1 M ionic strength 2:1 electrolyte was used; the hard sphere ion radius was fixed at 2 Å). As follows from the comparison, the increase of the Stern layer thickness results in the corresponding shift of curves away from the macromolecule's surface.

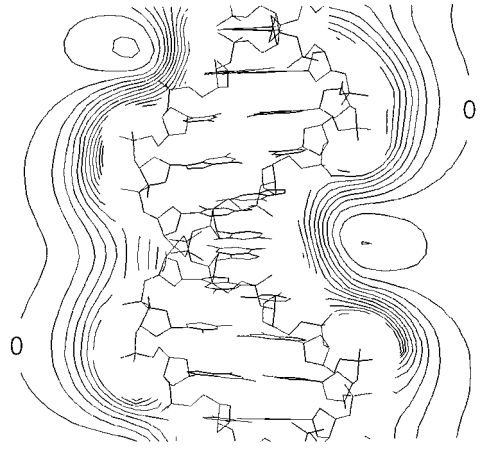

FIGURE 4 Contour map of the electrostatic potential shown in a plane slice across the helical axis. The model corresponds to Fig. 2 *Bc* where the plane is marked as line (3,4). Contours are taken with 0.25 *kT*/*e* difference and shown within the solvent-accessible area.

The influence of the macromolecule's dielectric constant ϵ to the ψ_{MPB} is surprisingly weak. For 0.5 M ionic strength 2:1 electrolyte, the difference between two electrostatic potentials obtained at ϵ = 10 and at ϵ = 80 reaches 0.5 *kT*/*e* on the ion-accessible surface of DNA. We can conclude that the image interactions do not play a significant role at the relatively high ionic strength because of the strong charge screening. In contrast, the ion-ion correlations and finite size of ions appear to be an important contributor to the electrostatic potential around a molecule of DNA, especially for multivalent electrolytes.

The physical meaning of this phenomenon is clear if one considers the first and the third terms of the PMF in Eq. 1. Let us consider a counterion (i.e., a cation in the case of DNA) at some position in the averaged diffuse cloud of electricity around DNA. There the cation appears to be surrounded by the cloud of the same sign charges. The ion-ion correlations mean that these diffuse charges are themselves locally repelled from the cation because of electrostatic interactions. This repulsion obviously decreases the

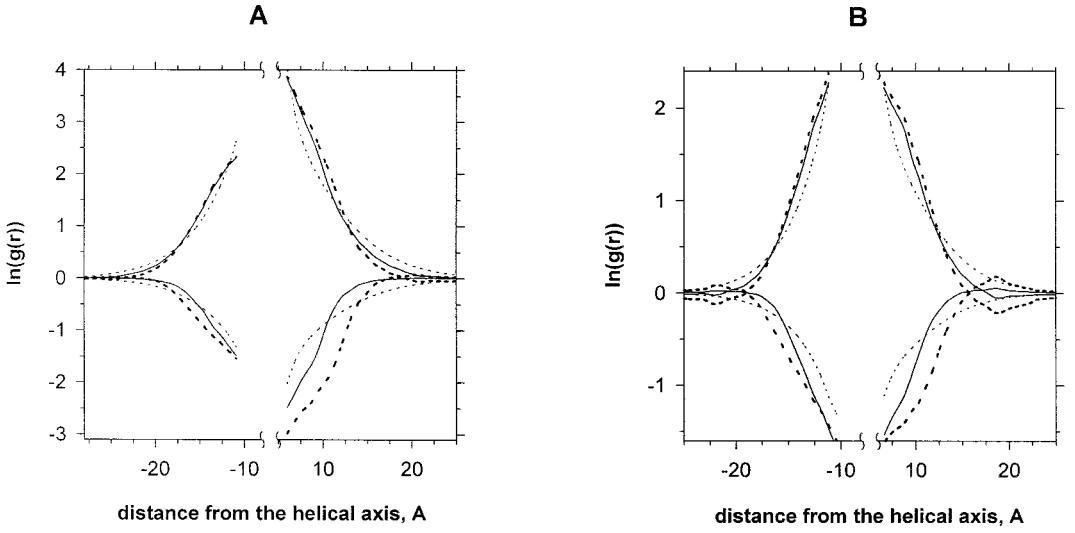

FIGURE 5 Plots of ionic distributions around the all-atom model of DNA; 2:1 electrolyte at $I = 0.5$ M (*A*) and at $I = 1$ M (*B*). Profiles are taken along line (1,2) marked in Fig. 2. The thin dotted curves are calculated via solution of the PB equation; the solid and thick dotted curves correspond to the MPB results for $d_{ion} = 4$ Å and $d_{ion} = 6$ Å, respectively.

electrostatic potential at the cation and, consequently, the electrostatic energy of the cation. The higher the local mean concentration of surrounding counterions, the higher this additional decrease of energy of each counterion. As a result, the ion-ion interactions produce an attraction of counterions by the area of higher counterion concentration in addition to the mean electric field force. Such attractive forces act also on a co-ion (anion) that appears to be surrounded by the cloud of opposite-sign electricity. The anion attracts these positive charges, which also decreases its electrostatic energy. Thus, one contribution to the third PMF term $q_\alpha \int_0^1 d\lambda \{\eta_\alpha(\mathbf{r}|\lambda) - \eta_\alpha(\infty|\lambda)\}$ from Eq. 1 should be negative for both co- and counterions. It can be shown that a value of this contribution is proportional to the square of the ion valency. The second contribution, implicitly involved in the integral, originates from the finite size of an ion. Indeed, putting an ion (together with surrounding zone of ionic exclusion) into the diffuse cloud of electricity is equivalent to neutralization of the diffuse charge within the ionic excluded volume, which is equivalent to filling this volume with diffuse charge of the opposite sign and of the same density. The potential at the counterions is obviously decreased by the potential of this compensating charge, because of opposite signs. In contrast, the absolute value of the potential at the co-ions is increased. In other words, the second contribution, implicitly involved in the integral, describes an additional attraction of counterions by the area of high ion mean concentration and a corresponding repulsion of co-ions from this area. It can be shown that this second contribution to the integral is proportional to the ion valency. Finally, one should expect that the value of the integral is always negative for counterions, is partly compensated for co-ions, and strongly depends on the ion valency. The volume exclusion term of the PMF (that is, $kT\ln\xi_\alpha(\mathbf{r})$ from Eq. 1) always represents the positive work to insert both anions and cations into the averaged ionic cloud around DNA; i.e., it always describes an addition repulsion of ions from the high ionic density area. Finally, one has to conclude that the strong additional attraction of counterions together with asymmetrically lower additional forces acting on co-ions may cause an excess of counterions in the ionic cloud, i.e., the effect of overneutralization. The picture described above is clearly seen from the graphical representation of separate contributions to the PMF, shown in Fig. 6 as 1D plots of the PMF terms. The models correspond to Fig. 2 *B* (2:1 electrolyte; $I = 0.5$ M). One can see that the mean electrostatic potential originates from a sophisticated balance of forces that may be notably higher than the mean electric force even in the case of moderately diluted ($C = 0.167$ M) 2:1 electrolyte. The exclusion volume term is confirmed to be higher in the case of $d_{ion} = 6$ Å (Fig. 6 *B*) than that at $d_{ion} = 4$ Å (Fig. 6 *A*) and the predicted ratio of volume values $(6/4)^3 \approx 3.4$ is observed starting from a distance of ~11–12 Å. A strong additional attraction of counterions described by the third term on the right size of Eq. 1, as well as a low value of this term for co-ions, are also seen from Fig. 6.

The effect of interionic correlations is pronounced even for diluted multivalent electrolytes. Comparisons of ψ_{MPB} with ψ_{PB} for 2:1 and 1:1 electrolytes at $I = 0.05$ M ($\lambda_{DH} = 13.7$ Å) are shown in Fig. 7 as 1D profiles taken along direction (1,2) from Fig. 2. The all-atom model of the DNA dodecamer was mapped onto an $81 \times 81 \times 25$ cubic lattice. The lattice spacing is 1.4 Å, a number of Eqs. 3 within one loop (5)-(3)-(1)-(5) is approximately 16,000. In Fig. 7 *A*, a comparison of ψ_{MPB} with ψ_{PB} is shown within the ion-accessible area for 2:1 electrolyte ($d_{ion} = 4$ Å). No overneutralization is observed, but one can see a significant difference between the two potentials caused by the interionic correlations. Corresponding 1D solutions of the MPB and

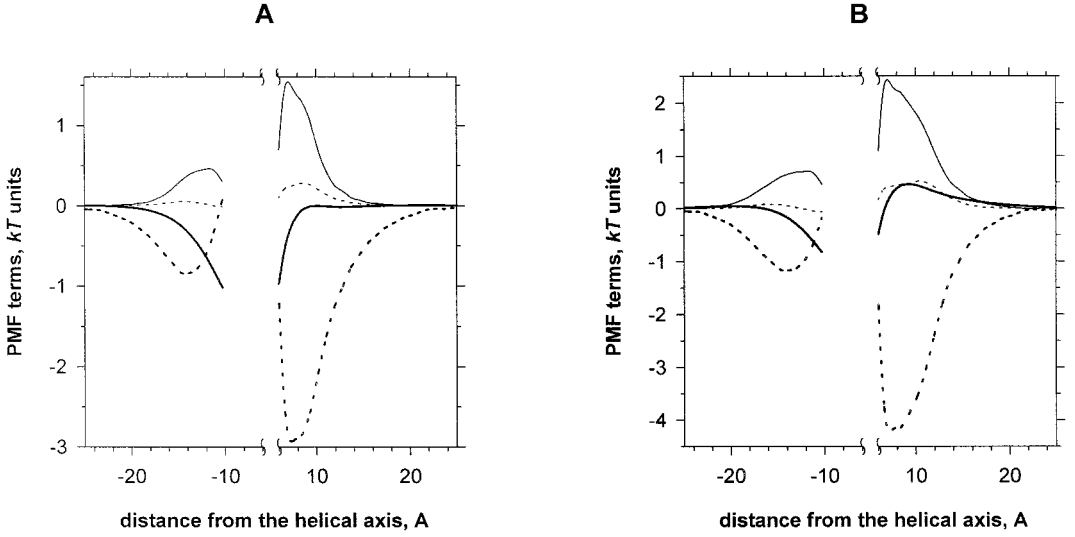

FIGURE 6 PMF terms plots for the models from Fig. 2, *Bb* and *Bc* (2:1 electrolyte; $I = 0.5$ M; $d_{ion} = 4$ Å (*A*) and $d_{ion} = 6$ Å (*B*)). Profiles are taken along line (1,2) marked in Fig. 2. The thin solid line represents the volume exclusion term. The thick dotted line corresponds to the third term of the PMF from Eq. 1 for counterions. The thin dotted line corresponds to the third term of the PMF for co-ions. The thick solid line represents $e\psi$ function.

PB equations for the cylindrical approximate model of the DNA are also shown in Fig. 7 *A*. Parameters of the cylindrical model are as described in Testing, except for the internal dielectric constant taken as 10 according to that of the 3D model of DNA. One can see that the cylindrical model is a reasonable approximation of DNA at such concentrations of electrolytes. As in the case of more concentrated electrolyte, the maximal influence of the geometry of DNA on potentials is observed in the vicinity of the major groove of DNA. For diluted 2:1 electrolyte this is the only region where ψ_{MPB} is found to be sensitive to the ionic diameter. Corresponding curves of ψ_{MPB} at $d_{ion} = 4$ Å and at $d_{ion} = 6$ Å are shown in Fig. 7 *B* where the data are presented within the solvent-accessible area. The difference in the potentials in the major groove originates from a corresponding difference in counterion distributions close to the ion-accessible surface and might be a numerical artifact because the FD grid resolution is comparable to the size of the region of maximal counterion condensation. In the case of a diluted 1:1 electrolyte, the PB approximation is con-

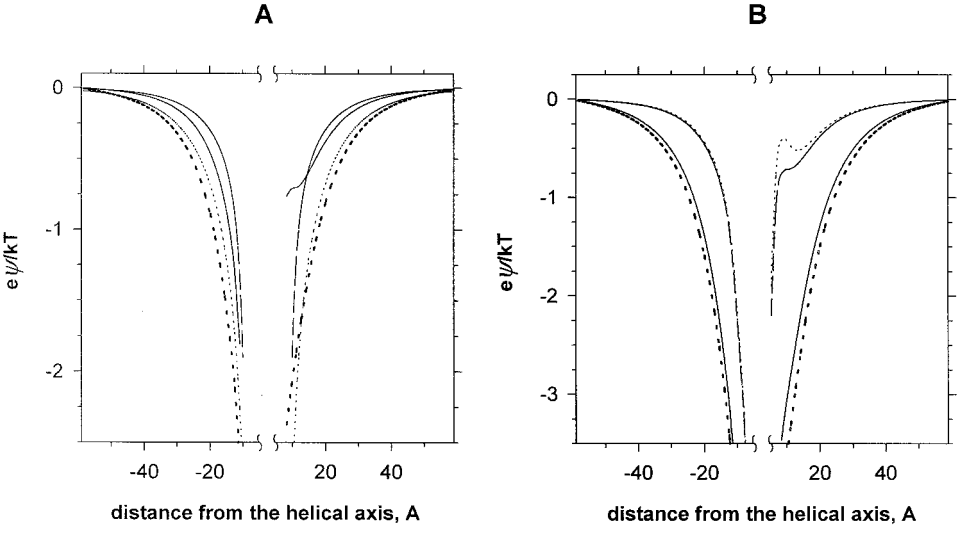

FIGURE 7 Plots of the electrostatic potential around DNA. Diluted solution of 2:1 and 1:1 electrolytes; $I = 0.05$ M ($C_{2:1} = 0.017$ M; $C_{1:1} = 0.05$ M). Profiles are taken along line (1,2) marked in Fig. 2. (*A*) 2:1 electrolyte; potentials are shown within the ion-accessible area. The thick dotted curve is a solution of the PB equation for the all-atom model of DNA; the solid curve is corresponding MPB results for $d_{ion} = 4$ Å. The thin dotted and dashed curves are PB and MPB results for the cylindrical approximate model of DNA. (*B*) All-atom model of DNA; 2:1 and 1:1 electrolytes; potentials are shown within the solvent-accessible area. The solid curve denotes a solution of the MPB equations for 1:1 electrolyte ($d_{ion} = 4$ Å); the thick dotted curve is the PB electrostatic potential for 1:1 electrolyte. The thin dotted and dashed curves are the MPB electrostatic potentials for 2:1 electrolyte obtained at $d_{ion} = 6$ Å and $d_{ion} = 4$ Å, respectively.

firmed to be satisfactory for DNA. Corresponding 1D profiles of ψ_{MPB} and ψ_{PB} at $C_{1:1} = 0.05$ M are also shown in Fig. 7 *B*. The difference is within several percent.

Despite the above mentioned sensitivity of electrostatic potentials to the finite size of ions for a multivalent electrolyte, the difference of the PB and MPB electrostatic potentials at the macromolecular atoms does not seem to be so dramatic. All evaluations of the integral $\frac{1}{2}\int\rho_0(\psi_{PB} - \psi_{MPB})d^3\mathbf{r}$ show that this value is less than 1.5 kJ/mol per nucleotide, which is obviously not too high. Besides, this maximal value is reached only for the 2:1 electrolyte. It is notably lower in the case of 1:1 salt. The difference is caused only by the mobile ion charge distribution, i.e., by differences in the ionic clouds in the two theories. Although completely determining the electrostatic potential at a significant separation from the macromolecule, this mobile ion distribution has a relatively weak effect on the potential at the macromolecular charged groups.

CONCLUSIONS

The numerical implementation of the MPB equations seems to be a natural extension of the FD algorithm for the PB equation. In fact, the simplest statistical mechanics approach is replaced by a more advanced one, and the same algorithm is applied to the new equations, which are quite similar. The new solution requires a lot of computations. Indeed, one has 20,000–50,000 or even more linearized boundary value problems (3) (together with a few problems (5)) instead of one nonlinear problem (5) in the case of the widely used PB equation. On the other hand, the time of computations can be drastically reduced by an increase of the number of processors, because all of these linearized problems can be solved in parallel within cycle (5)-(3)-(1)-(5). As mentioned above, the last requires only two to three iterations to obtain convergence. Further advances in parallel computing will permit the MPB calculations to be reduced into a time frame comparable to PB calculations. The finite-difference approach is not the only method to solve system (1)-(5) numerically. The finite element method (Johnson, 1987) seems to be promising.

Looking at Figs. 2–7, we have to conclude that the PB equation is a poor approximation in the case of multivalent electrolyte at moderate salt concentration. For such highly charged systems as DNA, it notably overestimates the absolute value of the potential at any distance from the macromolecule even for diluted multivalent electrolyte. Such a deviation is also pronounced for moderately diluted monovalent electrolyte at some distance from the macromolecule's surface (Fig. 3 *A*). This effect was clearly observed when the PB potentials near the surface of DNA were compared with the experimentally measured potentials (Hecht et al., 1995). The more advanced MPB equation should be applied to studies of the electrostatic contribution to DNA-ligand or DNA-protein interactions in the presence of multivalent ions or at relatively high concentrations of monovalent ions. It is important to note that only one new adjustable parameter, the size of ions, is used.

The calculations presented in this paper were executed thanks to the computational grant at the Interdisciplinary Modelling Center of Warsaw University.

REFERENCES

Antosiewicz, J., J. A. McCammon, and M. K. Gilson. 1994. Prediction of pH-dependent properties of proteins. *J. Mol. Biol.* 238:415–436.

Arakawa, T., and S. N. Timasheff. 1985. Theory of protein solubility. *Methods Enzymol.* 114:49–77.

Bashford, D., and M. Karplus. 1990. pK_a's of ionizable groups in proteins: atomic detail from a continuum electrostatic model. *Biochemistry.* 29: 10219–10225.

Bashford, D., and M. Karplus. 1991. Multiple-site titration curves of proteins: an analysis of exact and approximate methods for their calculation. *J. Phys. Chem.* 95:9556–9561.

Bell, G. M., and S. Levine. 1966. A modified Poisson-Boltzmann equation in electric double layer theory. *In* Chemical Physics of Ionic Solutions. B. E. Conway and R. G. Barradas, editors. Wiley, New York. 409–461.

Bhuiyan, L. B., and C. W. Outhwaite. 1994. The cylindrical electric double layer in the modified Poisson-Boltzmann theory. *Philos. Magazine B.* 69:1051–1058.

Bhuiyan, L. B., C. W. Outhwaite, and J. R. C. van der Maarel. 1996. Structure functions of rod-like DNA fragment and polystyrenesulfonate solutions in the modified Poisson-Boltzmann theory. *Phys. A.* 231: 295–303.

Carnie, S. L., and G. M. Torrie. 1984. The statistical mechanics of the electrical double layer. *Adv. Chem. Phys.* 56:141–253.

Das, T., D. Bratko, L. B. Bhuiyan, and C. W. Outhwaite. 1995. Modified Poisson-Boltzmann theory applied to linear polyelectrolyte solutions. *J. Phys. Chem.* 99:410–418.

Das, T., D. Bratko, L. B. Bhuiyan, and C. W. Outhwaite. 1997. Polyelectrolyte solutions containing mixed valency ions in the cell model: a simulation and modified Poisson-Boltzmann study. *J. Chem. Phys.* 107: 9197–9207.

Degreve, L., and M. Lozada-Cassou. 1995. Monte Carlo and HNC/MSA results for an asymmetrical electrolyte in an external electric field of spherical geometry. *Mol. Phys.* 86:759–768.

Gavryushov, S., and P. Zielenkiewicz. 1997a. Multivalent ion distribution around a cylindrical polyion: contribution of polarization effects due to difference between dielectric properties of the macromolecule's interior and the aqueous solvent. *J. Phys. Chem. B.* 101:792–797.

Gavryushov, S., and P. Zielenkiewicz. 1997b. Electrostatic potential and free energy of proteins: a comparison of the Poisson-Boltzmann and the Bogolyubov-Born-Green-Yvon equations. *J. Phys. Chem. B.* 101: 10903–10909.

Hecht, J. L., B. Honig, Y.-K. Shin, and W. L. Hubbell. 1995. Electrostatic potentials near the surface of DNA: comparing theory and experiment. *J. Phys. Chem.* 99:7782–7786.

Jayaram, B., K. A. Sharp, and B. Honig. 1989. The electrostatic potential of B-DNA. *Biopolymers.* 28:975–993.

Johnson, C. 1987. Numerical Solution of Partial Differential Equations by the Finite Element Method. Cambridge University Press, Cambridge.

Lamm, G., and G. R. Pack. 1997. Calculation of dielectric constants near polyelectrolytes in solution. *J. Phys. Chem. B.* 101:959–965.

Lamm, G., L. Wong, and G. R. Pack. 1994. Monte Carlo and Poisson-Boltzmann calculations of the fraction of counterions bound to DNA. *Biopolymers.* 34:227–237.

Levine, S., and G. M. Bell. 1960. Theory of a modified Poisson-Boltzmann equation. I. The volume effect of hydrated ions. *J. Phys. Chem.* 64: 1188–1195.

Levine, S., and C. W. Outhwaite. 1978. Comparison of theories of the aqueous electric double layer at a charged plane interface. *J. Chem. Soc. Faraday Trans. 2.* 74:1670–1689.

Loewenthal, R., J. Sancho, T. Reinikainen, and A. R. Fersht. 1993. Long-range surface charge-charge interactions in proteins: comparison of experimental results with calculations from a theoretical method. *J. Mol. Biol.* 232:574–583.

Luty, B. A., M. E. Davis, and J. A. McCammon. 1992. Solving the finite-difference non-linear Poisson-Boltzmann equation. *J. Comp. Chem.* 13: 1114–1118.

Mills, P., C. F. Anderson, and M. T. Record, Jr. 1985. Monte Carlo studies of counterion-DNA interactions: comparison of the radial distribution of counterions with predictions of other polyelectrolyte theories. *J. Phys. Chem.* 89:3984–3994.

Misra, V. K., J. L. Hecht, K. A. Sharp, R. A. Friedman, and B. Honig. 1994a. Salt effects on protein-DNA interactions: the λcI repressor and *Eco*RI endonuclease. *J. Mol. Biol.* 238:264–280.

Misra, V. K., and B. Honig. 1995. On the magnitude of the electrostatic contribution to ligand-DNA interactions. *Proc. Natl. Acad. Sci. U.S.A.* 92:4691–4695.

Misra, V. K., and B. Honig. 1996. The electrostatic contribution to the B to Z transition of DNA. *Biochemistry.* 35:1115–1124.

Misra, V. K., K. A. Sharp, R. A. Friedman, and B. Honig. 1994b. Salt effects on ligand-DNA binding: minor groove binding antibiotics. *J. Mol. Biol.* 238:245–263.

Montoro, J. C. G., and J. L. F. Abascal. 1995. Ionic distribution around simple DNA models. I. Cylindrically averaged properties. *J. Chem. Phys.* 103:8273–8284.

Murthy, C. S., R. J. Bacquet, and P. J. Rossky. 1985. Ionic distributions near polyelectrolytes: a comparison of theoretical approaches. *J. Phys. Chem.* 89:701–710.

Oberoi, H., and N. M. Allewell. 1993. Multigrid solution of the nonlinear Poisson-Boltzmann equation and calculation of titration curves. *Biophys. J.* 65:48–55.

Outhwhaite, C. W. 1978. Modified Poisson-Boltzmann equation in electric double layer theory based on the Bogoliubov-Born-Green-Yvon integral equations. *J. Chem. Soc. Faraday Trans. 2.* 74:1214–1221.

Outhwaite, C. W., and L. B. Bhuiyan. 1991. A modified Poisson-Boltzmann analysis of the electric double layer around an isolated spherical macroion. *Mol. Phys.* 74:367–381.

Schaefer, M., M. Sommer, and M. Karplus. 1997. pH-dependence of protein stability: absolute electrostatic free energy differences between conformations. *J. Phys. Chem. B.* 101:1663–1683.

Soumpasis, D. M. 1984. Statistical mechanics of the B→Z transition of DNA: contribution of diffuse ionic interactions. *Proc. Natl. Acad. Sci. U.S.A.* 81:5116–5120.

Takahashi, T., H. Nakamura, and A. Wada. 1992. Electrostatic forces in two lysozymes: calculation and measurements of histidine pKa values. *Biopolymers.* 32:897–909.

Weiner, S. J., P. A. Kollman, D. A. Case, U. C. Singh, C. Ghio, G. Alagona, S. Profeta, Jr., and P. Weiner. 1984. A new force field for molecular mechanical simulation of nucleic acids and proteins. *J. Am. Chem. Soc.* 106:765–784.

Young, M. A., B. Jayaram, and D. L. Beveridge. 1997a. Intrusion of counterions into the spine of hydration in the minor groove of B-DNA: fractional occupancy of electronegative pockets. *J. Am. Chem. Soc.* 119:59–69.

Young, M. A., G. Ravishanker, and D. L. Beveridge. 1997b. A 5-nanosecond molecular dynamics trajectory for B-DNA: analysis of structure, motions, and solvation. *Biophys. J.* 73:2313–2336.

Zacharias, M., B. A. Luty, M. E. Davis, and J. A. McCammon. 1992. Poisson-Boltzmann analysis of the λ repressor-operator interaction. *Biophys. J.* 63:1280–1285.